Analysis of experimental data on neutron scattering from superfluid helium at large momentum transfers*

L. J. Rodriguez† and H. A. Gersch
School of Physics, Georgia Institute of Technology, Atlanta, Georgia 30332
H. A. Mook
Solid State Division, Oak Ridge National Laboratory, Oak Ridge, Tennessee 37830
(Received 17 September 1973)

In previous work an expression was developed which partially incorporates the effect of final-state interactions on thermal-neutron scattering from a many-body system. This expression is evaluated for a liquid He^4 target at momentum transfers of 14.3 and 28.6 $Å^{-1}$. The experimental results of Mook, Scherm, and Wilkinson for the scattering of neutrons from liquid helium are analyzed in terms of (a) a modified impulse approximation which includes final-state corrections only in the condensate contribution to the scattering and (b) an approximation which includes final-state effects on both condensate and noncondensate contributions to the scattering. These calculations substantiate a previous empirical assessment of the condensate portion of the scattering [(2.4 ± 1)%] and suggest that certain barely discernible features of the experimental scattering are real structures in the condensate contribution attributable to the structure of the liquid and the interaction potential of the helium atoms. Other helium properties deduced from the data at 1.2 and 4.2 °K are single-particle momentum distribution, one-particle density matrix, and mean kinetic energy of the helium atoms. These quantities are compared with predictions from existing Monte Carlo numerical studies of the ground state of He^4.

I. INTRODUCTION

The inelastic scattering cross section for neutrons on He^4 liquid is given in the Born approximation[1] by

$$\frac{d^2\sigma}{d\Omega d\mathcal{E}_f} = \frac{\sigma_b k_f}{4\pi\hbar k_i} S(k,\omega) \quad , \tag{1}$$

where $\hbar\vec{k} = \hbar\vec{k}_i - \hbar\vec{k}_f$ is the momentum transferred to the helium, $\hbar\omega = \mathcal{E}_i - \mathcal{E}_f$ is the energy transfer, $\sigma_b = 1.13$ b,[2] and $S(k,\omega)$ is the dynamic structure factor. For scattering from superfluid helium at large momentum transfer it is expected that the dynamic structure factor will be decomposable into a contribution from the condensate and a contribution from the noncondensate. If both the condensate fraction n_0 and the momentum transfer are sufficiently large, one could hope to experimentally resolve the scattering into a two-part distribution, a narrow peak contributed by the condensate superimposed on a broader peak arising from the noncondensate.

A recent paper[3] reported the results of a search for a Bose-Einstein condensation in superfluid helium utilizing inelastic neutron scattering with a typical momentum transfer of $k = 14.3$ $Å^{-1}$. Although a cursory inspection of the data does not show a two-part distribution, the results indicated structure in the dependence of the scattering cross section on energy loss which was interpretated as direct evidence for the existence of macroscopic occupation of the single-particle momentum state $p = 0$. In addition, it was found that a least-squares analysis could resolve the scattering data into a two-part distribution. This analysis fits the energy dependence of the measured dynamic structure factor[4] with the function

$$I(\omega) = A_0 + A_1 e^{-(\omega - A_2)^2/A_3^2} + A_4 e^{-(\omega - A_5)^4/A_6^4} + A_7 e^{-(\omega - A_8)^2/A_9^2} \quad , \tag{2}$$

where $A_0, A_1, \ldots, A_9$ were parameters found by the least-squares criteria of the data taken with the helium at a temperature of 1.2°K. The data at 4.2°K were fitted by a function of the same form except that A_7 was taken as zero; refer to Figs. 1 and 2 and Table I. The first term in Eq. (2) was interpretated as the background neutron count. The sum of the second and third terms was taken as proportional to the noncondensate contribution to the dynamic structure factor. The fourth term was identified with the condensate contribution. This interpretation of the data yields a condensate fraction of (2.4 ± 1)%.[5]

The present work is aimed at evaluating the width and shape of the condensate portion of the scattering and at extracting properties of the helium liquid from this experiment. The analysis is based on the following form of the dynamic structure factor, developed previously[6]:

$$S(k,\omega)=\sum_p n_p R\left(k,\omega-\omega_k-\frac{\vec{V}_k\cdot\vec{p}}{\hbar}\right), \tag{3}$$

where n_p is the single-particle momentum distribution (the fraction of atoms carrying momentum p), m is the helium mass, $\omega_k=\hbar k^2/2m$, $\vec{V}_k=\hbar\vec{k}/m$, and the function R,

$$2\pi R\left(k,\omega-\omega_k-\frac{\vec{p}\cdot\vec{V}_k}{\hbar}\right)=\int_{-\infty}^{\infty} dt\, e^{-i(\omega-\omega_k-\vec{p}\cdot\vec{V}_k/\hbar)t}R(k,t) \tag{4}$$

incorporates final-state effects on the scattering. The function $R(k,t)$ may be approximately evaluated from Eq. (37) of Ref. 6:

$$R(\vec{k},t)\cong\exp\left\{-\int\rho_2(\vec{r},0;\vec{r}+\vec{V}_k t,0)\left[1-\exp\left(i\int_0^t\{V[\vec{r}+\vec{V}_k(t-t')]-V(\vec{r}+\vec{V}_k t)\}dt'\right)\right]d\tau\Big/\rho_1(0,\vec{V}_k t)\right\}, \tag{5}$$

where $\rho_1(0,\vec{V}_k t)$ and $\rho_2(\vec{r},0,\vec{r}+\vec{V}_k t,0)$ are the liquid's one-particle and two-particle off-diagonal density matrices, respectively, and $\hbar\equiv 1$. For sufficiently large momentum transfer, $R(k,\omega-\omega_k-\vec{p}\cdot\vec{V}_k)$ should approach a δ function. In this limit Eq. (3) becomes the impulse approximation

$$S^{\mathrm{IA}}(k,\omega)=\sum_p n_p\,\delta(\omega-\omega_k-\vec{V}_k\cdot\vec{p}). \tag{6}$$

Assuming there is a Bose-Einstein condensation ($n_0\neq 0$), Eq. (3) becomes

$$S(k,\omega)=\frac{1}{(2\pi)^3\rho}\int dp^3 n_p R(k,\omega-\omega_k-\vec{V}_k\cdot\vec{p})+n_0 R(k,\omega-\omega_k) \tag{7}$$

and the impulse approximation becomes

$$S^{\mathrm{IA}}(k,\omega)=\frac{1}{4\pi^2\rho V_k}\int_{|\Omega|}^{\infty} dp\, p n_p+n_0\delta(\omega-\omega_k), \tag{8}$$

where n_0 is the condensate fraction, $\Omega=(\omega-\omega_k)/V_k$, and ρ is the helium number density.

A slight generalization of the impulse approximation will increase the range of momentum transfer over which it is a good approximation. This modification is the replacement of the δ-function condensate contribution by the R function

$$S^{\mathrm{IA}}(k,\omega)=\frac{1}{4\pi^2\rho V_k}\int_{|\Omega|}^{\infty} dp\, p n_p+n_0 R(k,\omega-\omega_k). \tag{9}$$

This approximation will be useful for those values of k for which the width of the R function is narrow compared to the width of n_p, allowing the replacement of R by a δ function in the integrated term of Eq. (7) even though the condensate term may have measurable width. In subsequent discussion Eq. (9) will be referred to as the impulse approximation. It includes the effect of final-state interactions on the condensate portion via the R function but neglects these effects on the noncondensate part.

In Sec. II the function $R(k,v_k\Omega-\vec{V}_k\cdot\vec{p})$ is evaluated and compared to the Gaussian form for the condensate portion of the scattering given in Eq. (2) and utilized in Ref. 3. In Sec. III the modified impulse approximation [Eq. (9)] is used to analyze

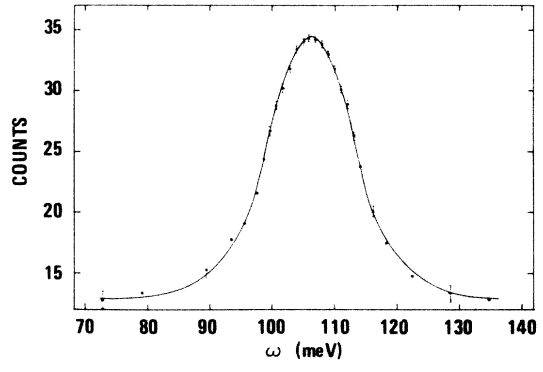

FIG. 1. $S(k,\omega)$ for He^4 at 1.2 °K. The circles are the experimental data, Ref. 3; and the solid line is the empirical fit $I(\omega)$, Eq. (2) and Table I. The units of the abscissa are neutron counts normalized to approximately 20 min of counting time per point.

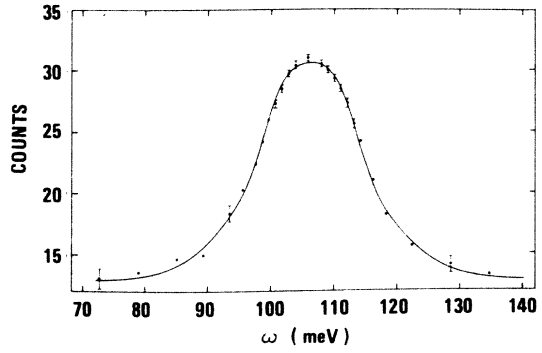

FIG. 2. $S(k,\omega)$ for He^4 at 4.2 °K. The circles are the experimental data, Ref. 3; and the solid line is the empirical fit $I(\omega)$, Eq. (2) and Table I. The units of the abscissa are neutron counts normalized to approximately 20 min of counting time per point.

the noncondensate portion of the scattering data yielding the following properties of the helium liquid at temperatures of 1.2 and 4.2°K: the single-particle momentum distribution for the atoms not in the condensate, the spatial dependence of the one-particle density matrix, and the mean kinetic energy per helium atom. These results are compared with corresponding predictions from existing Monte Carlo calculations on ground state of superfluid helium. Section IV contains an analysis of the noncondensate portion of the scattering data when final-state effects embodied in the R function are included. Qualitative estimates of these effects on the single-particle momentum distribution and quantitative estimates of these effects on the single-particle density matrix are given in that section. Section V contains a discussion of the results obtained.

II. EVALUATION OF FINAL-STATE EFFECTS

The evaluation of the R function is the central problem of this approach to the analysis of neutron scattering. $R(k, V_k\Omega - \vec{V}_k\cdot\vec{p})$ evaluated for $p=0$ is proportional to the condensate contribution to the dynamic structure factor, and when properly convoluted with the momentum distribution [refer to Eq. (7)] it yields the noncondensate part. In order to evaluate the R function in a straightforward manner, it is necessary to select forms for the helium-helium interaction potential $V(r)$, the one-particle density matrix $\rho_1(0, \vec{V}_k t)$, and the two-particle density matrix $\rho_2(\vec{r}, 0; \vec{r}+\vec{V}_k t, 0)$.

The results obtained here used the Lennard-Jones potential $V(r)$ to represent the helium-helium interaction

$$V(r) = 4\mathcal{E}[(\sigma/r)^{12} - (\sigma/r)^6], \tag{10}$$

TABLE I. Parameters from Eq. (2) obtained by least-squares fitting of the measured data. Parameters giving peak heights are in counts per run and parameters representing peak widths or positions are in millivolts. Width parameters are left unmultiplied by 2 ln2 so that they can be directly compared with the measured full width at half-maximum of $S(k,\omega)$.

Parameters	1.2 °K	4.2 °K
A_0	12.90	12.90
A_1	12.47	11.97
A_2	106.22	106.22
A_3	$20.76/2\ (\ln 2)^{1/2}$	$23.28/2\ (\ln 2)^{1/2}$
A_4	7.48	5.69
A_5	106.22	106.22
A_6	$12.82/2\ (\ln 2)^{1/4}$	$13.48/2\ (\ln 2)^{1/4}$
A_7	1.60	0.0
A_8	106.22	...
A_9	$4.92/2\ (\ln 2)^{1/2}$	...

with $\mathcal{E}=10.22$°K and $\sigma=2.556$ Å.[7] The selection of the two-particle density matrix was based on the following considerations. Viewing ρ_2 as a scalar product in $(N-2)$-particle Fock space

$$\rho_2(\vec{r}, 0; \vec{r}+\vec{V}_k t, 0) = \langle\varphi_0|\Psi^\dagger(\vec{r})\Psi^\dagger(0)\Psi(\vec{r}+\vec{V}_k t)\Psi(0)|\varphi_0\rangle,$$

where the helium is assumed to be in the ground state φ_0; the Schwartz inequality yields

$$|\rho_2| \le \langle\varphi_0|\Psi^\dagger(\vec{r})\Psi^\dagger(0)\Psi(0)\Psi(\vec{r})|\varphi_0\rangle^{1/2} \times\langle\varphi_0|\Psi^\dagger(0)\Psi^\dagger(\vec{r}+\vec{V}_k t)\Psi(\vec{r}+\vec{V}_k t)\Psi(0)|\varphi_0\rangle^{1/2}.$$

Assuming that the ground state can be represented by an everywhere positive wave function, ρ_2 is positive and the absolute value symbol may be removed, so that

$$\rho_2(\vec{r}, 0; \vec{r}+\vec{V}_k t, 0) \le \rho^2 g^{1/2}(\vec{r}) g^{1/2}(\vec{r}+\vec{V}_k t), \tag{12}$$

where $g(r)$ is the pair correlation function. When $t=0$, the inequality in Eq. (11) becomes an equality; therefore we expect $\rho^2 g^{1/2}(r) g^{1/2}(\vec{r}+\vec{V}_k t)$ to be a good approximation to ρ_2 for small values of t and all values of r.

For large values of $(\vec{r})$ and $(\vec{r}+\vec{V}_k t)$ we expect ρ_2 to be given by the Hartree-Fock approximation

$$\rho_2(\vec{r}, 0; \vec{r}+\vec{V}_k t, 0) \cong \rho\rho_1(\vec{r}, \vec{r}+\vec{V}_k t) + \rho_1(\vec{r}, 0)\rho_1(0, \vec{r}+\vec{V}_k t). \tag{13}$$

For most choices of $(\vec{r})$ and $(\vec{r}+\vec{V}_k t)$, the direct term $\rho\rho_1(\vec{r}, \vec{r}+\vec{V}_k t)$ will dominate the exchange term $\rho_1(\vec{r}, 0)\rho_1(0, \vec{r}+\vec{V}_k t)$, since $\rho_1(0, R) = \rho_1(R, 0) \approx \rho n_0$ for $R \gtrsim 4$ Å (refer to Fig. 9). Neglecting the exchange term, the approximation we take for ρ_2 which agrees with Eqs. (12) and (13) in their regions of applicability is

$$\rho_2(\vec{r}, 0; \vec{r}+\vec{V}_k t, 0) \approx \rho g^{1/2}(\vec{r}) g^{1/2}(\vec{r}+\vec{V}_k t)\rho_1(0, \vec{V}_k t), \tag{14}$$

where translational invariance has been used to replace $\rho_1(\vec{r}, \vec{r}+\vec{V}_k t)$ by $\rho_1(0, \vec{V}_k t)$. Estimates indicate that $g^{1/2}(r)$ is essentially zero for $r \lesssim 2$ Å, then rises sharply to approach unity at $r \approx 3$ Å, and exhibits rapidly damped oscillations about unity for $r \gtrsim 3$ Å.[7] To simplify the calculation somewhat we replace $g^{1/2}(r)$ by a unit step function, yielding

$$\rho_2(\vec{r}, 0; \vec{r}+\vec{V}_k t, 0) \approx \rho\Theta(|\vec{r}| - r_0) \times\Theta(|\vec{r}+\vec{V}_k t| - r_0)\rho_1(0, \vec{V}_k t), \tag{15}$$

where $\Theta(|r| - r_0) = 1$ for $|r| > r_0$, zero otherwise. In Eq. (15), r_0 is treated as a parameter which may be adjusted slightly under the restriction that $\Theta(|r| - r_0)$ remains a reasonable approximation to

$g^{1/2}(r)$. Since only the ratio $\rho_2(\vec{r},0;\vec{r}+\vec{V}_k t,0)/\rho_1(0,\vec{V}_k t)$ appears in Eq. (5), the above approximation for ρ_2 removes the need to chose a form for ρ_1.

The above approximation to the two-particle density matrix [Eq. (15)] is most appropriate for zero temperature because of the assumption that the state of the helium liquid is described by an everywhere positive wave function. The R-function calculation using this approximation will be compared with data taken at a helium temperature of 1.2°K. We are assuming that taking ρ_2 to be everywhere positive at 1.2°K introduces an error which is not incommensurably large compared to the error introduced by the other approximations used in obtaining Eq. (15).

Before proceeding it may be useful to make some comments about $R(k,t)$. By suitable manipulations of Eq. (5) it may be shown that for isotropic systems

$$R^*(k,t)=R(k,-t) \tag{16}$$

implying that the real part of $R(k,t)$ is an even function of t and that the imaginary part is an odd function of t. When Fourier transformed to yield $R(k,V_k\Omega)$, the real part of $R(k,t)$ will produce the even part (in Ω) of $R(k,V_k\Omega)$ and the imaginary part will yield the odd part of $R(k,V_k\Omega)$. If in turn $R(k,V_k\Omega)$ is convoluted with n_p in accordance with Eq. (3) to produce the noncondensate contribution to $S(k,\omega)$, the primary effect of the even part of $R(k,V_k\Omega)$ will be to modify the width of the dynamic structure factor and the main effect of the odd part will be to change the peak location from that of the impulse approximation.

Some general observations about the shape of $R(k,t)$ can be made more conveniently by considering the negative logarithm of R,

$$R(k,t)\equiv e^{-E(V_k t)}. \tag{17}$$

In our approximation $E(V_k t)$ is given by

$$E(V_k t)=\rho\int d\gamma^3\,\Theta(|\vec{\gamma}|-r_0)\,\Theta(|\vec{\gamma}+\vec{V}_k t|-r_0)\left[1-\exp\left(\frac{i}{V_k}\int_0^{V_k t} dy\,[V(\vec{\gamma}+\vec{y})-V(\vec{\gamma}+\vec{V}_k t)]\right)\right], \tag{18}$$

which is obtained from Eqs. (5) and (15) with the substitution $\vec{y}=\vec{V}_k(t-t')$ in one integral. A simple physical picture may be associated with mathematical operations called for in the evaluation of Eq. (18). In this picture a helium atom is struck by the incoming neutron at its initial position $\vec{r}$. The struck helium then travels along a straight line trajectory from its initial position $\vec{r}$ to its final position $(\vec{r}+\vec{V}_k t)$ at a velocity $\vec{V}_k$ and in a time t. During its "flight" the struck helium interacts with a single helium located at the origin of the coordinate system. We will loosely refer to this interaction as scattering of the struck helium. We will also loosely refer to a particular choice of initial position $\vec{r}$ as a configuration.

First note that the Lennard-Jones potential $V(r')$ being used in this calculation becomes highly repulsive as $|r'|$ decreases below r_0 (more precisely for $|r'|<\sigma=2.556$ Å, but $r_0\approx\sigma$) and that it is generally weakly attractive for $r_0\lesssim|r'|\lesssim R$, where R is some distance beyond which the potential is insignificantly small for the purposes of this calculation (in actual computations R was taken to be 8 Å though its value depends somewhat on k and t). Also note that the unit step functions in Eq. (18) remove all configurations for which the initial and/or final position is within the core defined by a sphere of radius r_0 about the origin of the coordinate system. This means that for small $V_k t$, $V_k t\ll 2r_0$; the hard repulsive part of the potential does not contribute to the scattering. The value of $E(V_k t)$ is therefore small, being determined by the weak attractive part of the potential.

For the repulsive part of the potential to contribute, the path of the struck particle, from $\vec{r}$ to $(\vec{r}+\vec{V}_k t)$, must pass completely through the core of radius r_0. As $V_k t$ approaches $2r_0$ these configurations begin to contribute and soon to provide the dominant portion of the value of $E(V_k t)$. For large $V_k t$ it can be shown that $E(V_k t)$ is dominated by a term linear in $V_k t$,

$$E(V_k t)\to[\tfrac{1}{2}\rho\sigma_{\text{tot}}+i4\pi(\rho/k)\,\text{Re}f(k,k)]\,V_k t+C', \tag{19}$$

where σ_{tot} is the total helium-helium cross section and $\text{Re}f(k,k)$ is the real part of the forward-scattering amplitude, both evaluated in the eikonal approximation, and C' is bounded. The term $\frac{1}{2}\rho\sigma_{\text{tot}}$ is just twice the reciprocal of a simple estimate of the mean free path and therefore this term is reminiscent of the results of phenomenological arguments which yield $V_k\rho\sigma_{\text{tot}}$ as an estimate of the width of the condensate portion of the scattering. It should be noted that the factor $\frac{1}{2}$ and the additive terms in Eq. (19) will make the width of $R(k,t)$ significantly different from the estimate $1/\rho\sigma_{\text{tot}}$.

The value of $E(V_k t)$ was determined by numerical integration of Eq. (18) for selected values of k, t, and r_0. The results for the real part of $E(V_k t)$ are shown in Fig. 3 and the imaginary part is shown in Fig. 4.

The real part of Eq. (18) appears to be well be-

haved with small computational error and so a smooth curve has been drawn through the computed points in Fig. 3. The imaginary part of Eq. (18) is not as smooth and there is noticeable error in its evaluation at large values of $V_k t$. For this reason, no attempt has been made to connect the computed values of the imaginary part by a curve, refer to Fig. 4. Where significant, the upper-half of the error bar (numerical error only) is shown for $k = 28.6$ Å^{-1}, $r = 2.5$ Å; and the lower-half of the bar for $k = 14.3$ Å^{-1}, $r = 2.5$ Å. A crude check of E in the region 8 Å $\lesssim V_k t \lesssim 10$ Å indicates that the slope of the real part of E corresponds to a total cross section [according to Eq. (19)] of ≈ 35 Å^2 for $k = 14.3$ Å^{-1} and ≈ 31 Å^2 for $k = 28.6$ Å^{-1}, in rough agreement with the experimentally measured cross section.[8]

Figure 5 contains $R(k, V_k\Omega)$ for selected values of k. Plotted in terms of Ω, the width of $R(k, V_k\Omega)$ narrows rather slowly as a function of k. From Eq. (9) it is evident that the width in terms of Ω of the noncondensate contribution evaluated in the impulse approximation is independent of k. The practical implication of this is that if an experiment performed at a given value of k is repeated with a slightly higher value of k one can only expect a very slight relative sharpening of the condensate portion over the noncondensate. This observation may be slightly ameliorated by the fact that the Lennard-Jones potential used in this calculation is known to be somewhat more repulsive than the actual helium-helium interaction for small distances.[8] Somewhat pessimistically, we do not expect much relief from this nuance for values of momentum transfer attainable with present experimental techniques.

On a more optimistic note, the function $R(k, V_k\Omega)$ shown in Fig. 5 exhibits a nonmonotonic behavior as a function of Ω. This characteristic is easily traced back to the short-time behavior of the function $E(V_k t)$ defined in Eq. (17) and exhibited in Figs. 3 and 4, which is radically different from the linear in $V_k t$ behavior given by Eq. (19) for long time. Clearly, this occurs because the struck helium particle initially finds itself in an environment of other helium atoms strongly conditioned by the liquid's local structure and can travel on the average some distance (~2–3 Å) before suffering significant collisions with other helium atoms.

Finally, Fig. 6 in this section presents our results for the condensate portion of $S(k, \omega)$ evaluated for the conditions corresponding to the experiment of Mook, Scherm, and Wilkinson. The condensate part of $S(k, \omega)$ was obtained from $n_0 R(k, V_k\Omega)$ assuming that the condensate fraction is 2.4%. Figure 6 also contains the best fitting Gaussian form for the condensate $A_7 \exp[-(\omega - A_8)^2/A_9^2]$, refer to Eq. (2), and that portion of the data judged to be

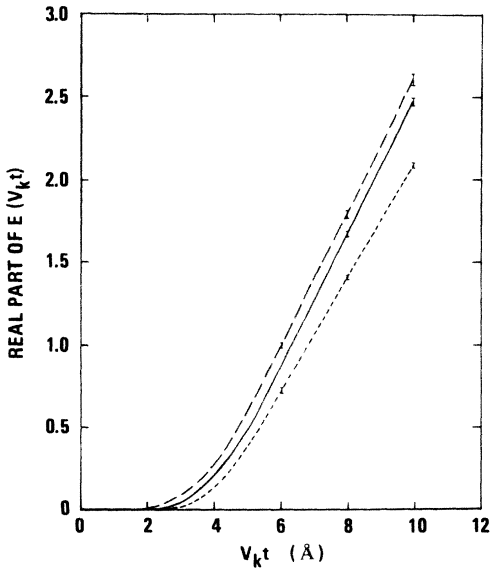

FIG. 3. Real part of $E(V_k t)$: solid line for $k = 14.3$ Å^{-1} and $r_0 = 2.5$ Å; long-dashed line $k = 14.3$ Å^{-1} and $r_0 = 2.4$ Å; short-dashed line $k = 28.6$ Å^{-1} and $r = 2.5$ Å. Errors indicated where significant.

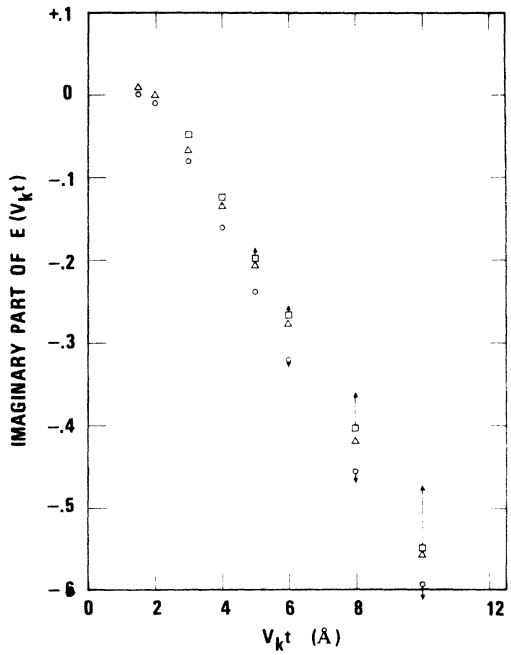

FIG. 4. Imaginary part of $E(V_k t)$: circles, $k = 14.3$ Å^{-1} and $r_0 = 2.5$ Å, lower-half of error bar shown; triangles, $k = 14.3$ Å and $r_0 = 2.4$ Å; squares, $k = 28.6$ Å^{-1} and $r_0 = 2.5$ Å, upper-half of error bar shown.

contributed by the condensate. The "condensate" part of the data was obtained by subtracting the first three terms of Eq. (2) from the actual data. The function $n_0 R(k, V_k\Omega)$ is approximately 17% wider than the best-fitting Gaussian form for the condensate (after the experimental resolution function has been deconvoluted from the Gaussian). The data may be able to support this extra width in $n_0 R(k, V_k\Omega)$. The peak location of $n_0 R(k, V_k\Omega)$ is approximately 1.2 meV higher than the best-fit location and approximately 0.5 meV higher than the peak of the impulse approximation. It is experimentally well established that the peak of the dynamic structure factor occurs at an energy loss slightly below the impulse approximation.[3,12] It appears that the physical mechanism(s) which dominate the determination of the peak location are not taken into account by the approximations being used here to evaluate $n_0 R(k, V_k\Omega)$. It is evident that if $n_0 R(k, V_k\Omega)$ were used in place of the "condensate" Gaussian in Eq. (2) that the best-fitting value for the condensate fraction would not be substantially different from the previous estimate[3] of $(2.4 \pm 1)\%$.

The structure in the energy dependence of the experimentally obtained dynamic structure factor is discernible in this figure in the vicinity of 101 and 111 meV. The function $n_0 R(k, V_k\Omega)$ also has structure which is suggestive of the structure in the data, but the structure in $n_0 R$ is located too far from the peak and is less dramatic. The structure in our evaluation of the condensate contribution could be made more pronounced by choosing a significantly larger value for r_0, but then the theta functions $\Theta(|r| - r_0)$ and $\Theta(|\vec{r} + \vec{V}_k t| - r_0)$ used in Eq. (15) would no longer be a reasonable approximation to $g^{1/2}(r)$ and $g^{1/2}(\vec{r} + \vec{V}_k t)$. A more precise evaluation of R, in particular the structure in its wings, will probably require a more accurate approximation to $\rho_2(\vec{r}, 0; \vec{r} + \vec{V}_k t, 0)$ than was used in this evaluation.

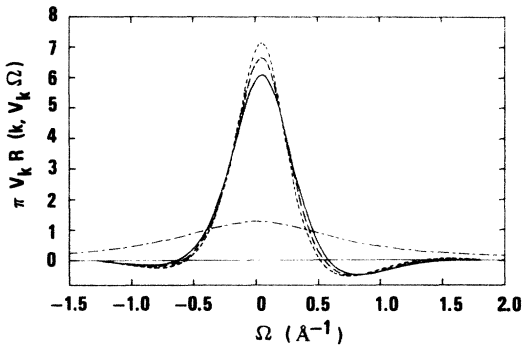

FIG. 5. $R(k, V_k\Omega)$ for $r_0 = 2.5$ Å: solid line, $k = 14.3$ Å^{-1}; long-dashed line $k = 28.6$ Å^{-1}; short-dashed line, $k = 57.2$ Å^{-1}; alternating long and short dashes, phenomenologically obtained Lorentzian with half-width at half-maximum of $\rho\sigma$. Helium number density taken to be $\rho = 0.022$ atoms Å^{-3}, helium-helium cross section taken to be $\sigma = 35$ Å^2. $\Omega = (\omega - \omega_k)/V_k$.

III. EXTRACTION OF HELIUM LIQUID PROPERTIES UTILIZING IMPULSE APPROXIMATION

Based on the analysis of the experimental data in Ref. 3 and the results of the analysis in Sec. II, we judge that the condensate contribution to the dynamic structure factor has a full width at half-maximum (FWHM) of approximately 5 meV at $k = 14.3$ Å^{-1}, while the FWHM of the noncondensate part is roughly 16 meV. In the formulation being used here the noncondensate part of the dynamic structure factor is given by

$$S_{NC}(k, \omega) = \frac{1}{(2\pi)^2 \rho} \int dp^3 n_p R(k, V_k\Omega - \vec{V}_k \cdot \vec{p}). \quad (20)$$

From the above discussion the FWHM of S_{NC} is approximately 16 meV while the width of R is roughly 5 meV. This suggests that the modified impulse approximation [Eq. (9)] may be used; recognizing that the final-state effects implied by the width of R will be small, though not necessarily negligible (see Sec. IV).

Using the impulse approximation, the extraction of the noncondensate contribution S_{NC} from the experimental data provides an input from which the single-particle momentum distributing the one-particle density matrix, the mean kinetic energy per atom in the helium liquid may be cal-

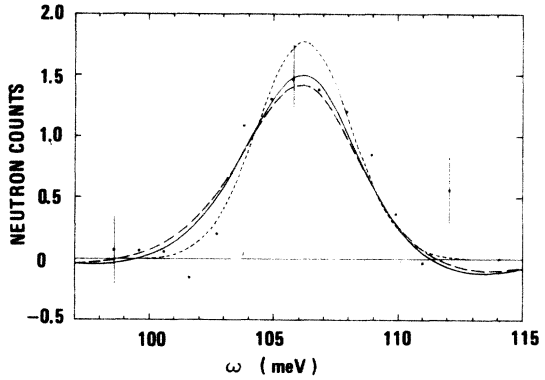

FIG. 6. Condensate contribution to the dynamic structure factor: circles, "condensate" portion of the data (see text); solid line, theoretical estimate of condensate portion taking $n_0 = 2.4\%$ and $r_0 = 2.5$ Å; long-dashed line, theoretical estimate of condensate portion taking $n_0 = 2.4\%$ and $r_0 = 2.4$ Å; short-dashed line, best-fit Gaussian with experimental resolution removed. The theoretical estimate has been arbitrarily translated in energy so that its peak coincides with experiment.

culated. This is discussed in this section.

Taking the partial derivative of the noncondensate part of Eq. (9) with respect to ω at constant k yields

$$\Omega n_\Omega = -(4\pi^2 \rho V_k^2)\left(\frac{\partial S_{NC}}{\partial \omega}\right)_k . \tag{21}$$

The experiment was conducted at constant scattering angle θ of 135°. The momentum transfer, energy transfer, and scattering angle are interrelated by

$$k^2(\theta, \omega) = 2M\{2\mathcal{E}_i[1 - (1 - \omega/\mathcal{E}_i)^{1/2}\cos\theta] - \omega\}, \tag{22}$$

where M is the neutron mass. Using Eqs. (9) and (22), a somewhat uninteresting exercise in partial derivatives leads to

$$\Omega n_\Omega = -4\pi^2 \rho V_k^2 \left[\left(\frac{\partial S_{NC}}{\partial \omega}\right)_\theta + \frac{S_{NC}}{k}\left(\frac{\partial k}{\partial \omega}\right)_\theta\right] \Big/ \left[1 - V_k\left(1 + \frac{\Omega}{k}\right)\left(\frac{\partial k}{\partial \omega}\right)_\theta\right], \tag{23}$$

where $\Omega = (\omega - \omega_k)/V_k$. As previously noted, the data, as presented in its final form in Ref. 3 and reproduced here, are proportional to the dynamic structure factor broadened by a resolution function with a FWHM of about 2.1 meV.

For convenience we choose to use the appropriate portion of the empirical fit Eq. (2) rather than the actual data points in the application of Eq. (23), i.e., we identify

$$C I_{NC}(\omega) \cong (\pi\Gamma)^{-1/2} \int_{-\infty}^{\infty} d\mathcal{E}\, e^{-(\omega - \mathcal{E})^2/\Gamma} S_{NC}(\theta, \omega), \tag{24}$$

where

$$I_{NC}(\omega) \equiv A_1 e^{-(\omega - A_2)^2/A_3^2} + A_4 e^{-(\omega - A_5)^4/A_6^4}, \tag{25}$$

$\Gamma = (2.1)^2/(4\ln 2)$ represents the width of the experimental resolution function, and C is a constant to be determined by normalizing the single-particle momentum distribution obtained from Eq. (23):

$$\sum_p n_p = 1. \tag{26}$$

The following approximation to the solution of Eq. (24) was used:

$$S_{NC}(\theta, \omega) \approx C[A_1' e^{-(\omega - A_2)^2/A_3'^2} + P(\omega)], \tag{27}$$

where

$$A_1' = A_1 A_3/A_3', \tag{28}$$

$$A_3' = (A_3^2 - \Gamma)^{1/2}, \tag{29}$$

$$P(\omega) = A_4 \sum_{n=0}^{4} \frac{1}{n!}\left(\frac{-\Gamma}{4}\right)^n \frac{d^{2n}}{d\omega^{2n}} e^{-(\omega - A_5)^4/A_6^4}. \tag{30}$$

As may be verified by direct substitution, the Gaussian term in Eq. (27) exactly reproduces the Gaussian in Eq. (24) after convolution with the resolution function. The polynomial $P(\omega)$ approximately reproduces the term $A_4 \exp[-(E - A_5)^4/A_6^4]$ of Eq. (24) after resolution broadening, as verified by numerical integration. The function $P(\omega)$ was obtained from the first five terms of an infinite series solution to an integral equation in the form of Eq. (24). This series solution is discussed in Appendix A. The effect of approximately deconvoluting the term $I_3 = A_4 \exp[-(\omega - A_5)^4/A_6^4]$ in Eq. (25), producing thereby the function $P(\omega)$ is illustrated in Fig. 7. Plotted in the figure as a solid line is the first derivative with respect to energy loss ω of the term I_3. The corresponding derivative of the deconvolution of this term $P(\omega)$ is indicated by the dotted line in the figure. The adequacy of the five-term approximation to $P(\omega)$ is tested by convoluting this $P(\omega)$ with the experimental Gaussian resolution function, which should

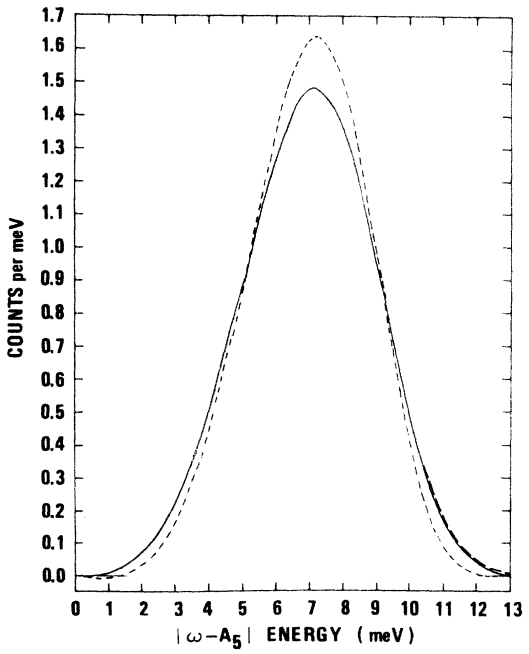

FIG. 7. Energy resolution correction: solid line, ω derivative of $A_4 \exp\{-[(\omega - A_5)/A_6]^4\}$; short-dashed line, ω derivative of $P(\omega)$, Eq. (30); long-dashed line, resolution-broadened ω derivative of $P(\omega)$ in region where it is distinguishable from solid line.

then reproduce the term I_3, or, as well, its ω derivative. Figure 7 shows that the results for $dP(\omega)/d\omega$ so convoluted (the dashed line in the figure) are graphically indistinguishable from $dI_3/d\omega$ except in the region $|\omega - A_5| \gtrsim 10.25$ meV.

The use of Eq. (27) in (23) yields the single-particle momentum distributions shown in Fig. 8. Along with the two distributions obtained in this analysis, Fig. 8 also contains the distribution found from a Monte Carlo calculation which assumed a Jastrow ground-state wave function.[7] To facilitate comparison with the Monte Carlo result, the n_p values determined from the experimental data have been normalized taking the helium density to be 0.022 atoms/Å^{-3} and the condensate fraction to be 0.11 at 1.2°K. Evident from the figure is the large number of atoms carrying a momentum $p \sim 0.7$ Å^{-1} which are not present in the Monte Carlo calculations. Of course, the momentum distributions n_p determined from this experiment corresponds to the temperatures 1.2 and 4.2°K, whereas the Monte Carlo calculations were performed for the ground state, $T = 0$°K. However, we do not think it likely that the differences in the n_p distributions at $T = 0$°K and $T = 1.2$°K shown in Fig. 8 are due to this difference in temperature.[9] Some insight into the possible source of this discrepancy is afforded by comparison of $\rho_1(0, r)$, the off-diagonal one-particle density matrix, related to n_p by

$$\rho_1(0, r) = \rho \sum_p n_p e^{i\vec{p}\cdot\vec{r}}. \tag{31}$$

For the Monte Carlo calculations, $\rho_1(0, r)$ is also related to the assumed form of the ground-state wave function $\Psi_g(r_1, r_2, \ldots, r_N)$ by

$$\rho_1(0, r) = \int \Psi_g(0, r_2, \ldots, r_N) \times \Psi_g(r, r_2, \ldots, r_N)\, dr_2 \cdots dr_N. \tag{32}$$

Figure 9 compares values for $\rho_1(0, r)$ from the experimentally determined n_p values with the Monte Carlo results. The excess atoms carrying momentum ~0.7 Å^{-1} in Fig. 6 give rise to the dip in $\rho_1(0, r)$ near $r \sim 6$ Å, resulting in a nonmonotonic $\rho_1(0, r)$, contrasted with the monotonically decreasing ρ_1 predicted by the computer studies. We believe that the monotonic behavior of $\rho_1(0, r)$ is due to the use, in Eq. (32), of a Jastrow ground-

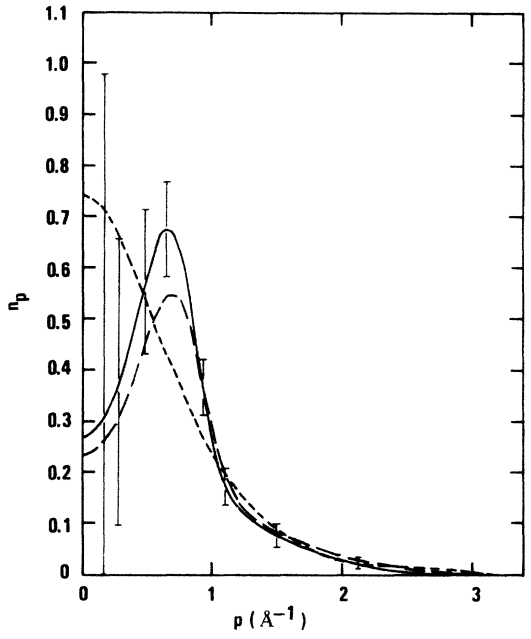

FIG. 8. Single-particle momentum distributions: solid line, distribution found from 1.2°K; long-dashed line, distribution found from 4.2°K data; short-dashed line, the result of a Monte Carlo calculation, Ref. 7. Estimated error shown for 1.2°K distribution. The behavior of the error bars at small values of p is explained by first noting that the error bars in pn_p are (approximately) directly proportional to the error in the experimentally determined slope of $S(k, \omega)$, refer to Eq. (21), and therefore of the same order of magnitude for the MSW experiment over the range of p. Secondly, note that the process of obtaining n_p by dividing pn_p by p "amplifies" the error for small values of p.

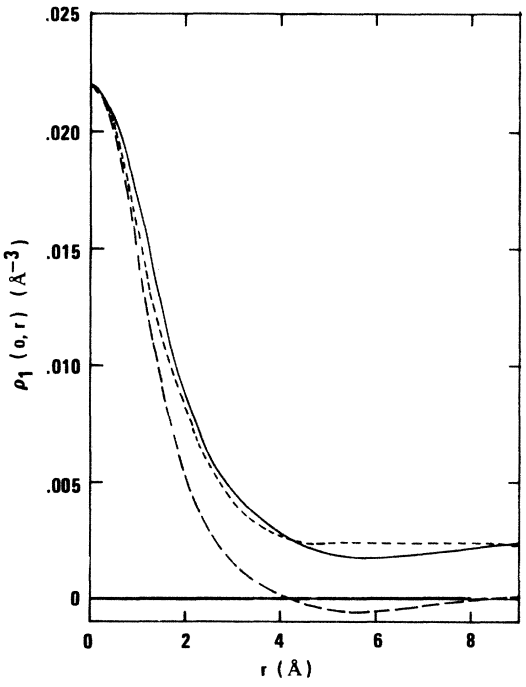

FIG. 9. Off-diagonal one-particle density matrix: solid line, obtained from 1.2°K data; long-dashed line, obtained from 4.2°K data; short-dashed line, result of Monte Carlo calculation, Ref. 7.

state wave function

$$\Psi(r^N) = \prod_{1 \le i < j \le N} f(r_{ij})$$

for which the assumed form of $f(r)$ is a monotonically increasing function of r, i.e., $f(r) = \exp[-(a/r)^5]$. Such an $f(r)$ does not account for attractive interactions, which should cause a "bump" in $f(r)$ at an r value roughly corresponding to the range of the attraction, e.g., $f(r) = \exp[-(a/r)^5 + (b/r)^m]$, $b > 0$, $m > 0$. Graphical estimates of $\rho_1(0, r)$ from Eq. (32) indicate that the bump in $f(r)$ can produce a nonmonotonic $\rho_1(0, r)$. We think it would be interesting to repeat the Monte Carlo calculations allowing for the effect of attractive interactions between the helium atoms[10] to see if nonmonotonic behavior of $\rho_1(0, r)$ results.

The mean kinetic energy per helium atom is readily obtained from the momentum distribution by calculating the mean-squared momentum. We obtain the results 12°K/atom at a temperature of 1.2°K and 16°K/atom at 4.2°K. Other estimates for this quantity obtained from Monte Carlo results for the ground state[7,11] or from experimental data at about 1°K (Ref. 12) range from 10.6 to 15.8°K/atom.

IV. FINAL-STATE EFFECTS ON THE NONCONDENSATE

In Sec. III final-state effects were ignored in obtaining the single-particle momentum distribution and related quantities. In this section we will discuss, somewhat qualitatively, the modification of previous results brought about by including the final-state effects embodied in the R function.

The starting point is an expression for the noncondensate contribution to Eq. (7),

$$S_{NC}(k, \omega) = \frac{1}{4\pi^2\rho} \int_0^\infty p^2\, dp\, n_p \times \int_{-1}^{1} dV\, R(k, V_k\Omega - V_k p V), \tag{33}$$

which has been written in terms of polar coordinates with the change of variable $V = \cos\theta'$, θ' the polar angle. To obtain a formula analogous to Eq. (21) one takes the partial derivative of Eq. (33) with respect to ω holding k constant

$$-4\pi^2\rho V_k \left(\frac{\partial S}{\partial \omega}\right)_k = \int_0^\infty dp\, p n_p R(k, V_k\Omega - V_k p) - \int_0^\infty dp\, p n_p R(k, V_k\Omega + V_k p). \tag{34}$$

The above equation can be written in a slightly more compact form by replacing p by $-p$ in the second integral and artifically extending the definition of n_p to negative values by the prescription $n_{-p} = n_p$. Equation (34) becomes

$$\int_{-\infty}^{\infty} dp\, p n_p R(k, V_k\Omega - V_k p) = -4\pi^2\rho V_k \left(\frac{\partial S}{\partial \omega}\right)_k. \tag{35}$$

The analogous formula for constant scattering angle θ is obtained by taking the partial derivative of Eq. (33) with respect to ω for constant θ using Eq. (22) to inter-relate k, ω, and θ. The result is

$$4\pi^2\rho V_k \left[\left(\frac{\partial S}{\partial \omega}\right)_\theta + \frac{1}{k} S^{NC} \left(\frac{\partial k}{\partial \omega}\right)_\theta\right] = \left[-1 + V_k \left(\frac{\partial k}{\partial \omega}\right)_\theta\right] \int_{-\infty}^{\infty} dp\, p n_p R(k, V_k\Omega - V_k p) + V_k \left(\frac{\partial k}{\partial \omega}\right)_\theta \int_{-\infty}^{\infty} dp\, \frac{p^2}{k}\, n_p R(k, V_k\Omega - V_k p) + V_k \left(\frac{\partial k}{\partial \omega}\right)_\theta \int_0^\infty dp\, p^2 n_p \frac{\partial R}{\partial k}, \tag{36}$$

where

$$\frac{\partial R}{\partial k} \equiv \left(\frac{\partial}{\partial k} R(k, V_k\Omega - V_k p)\right)_{V_k\Omega - V_k p}.$$

To proceed with determining n_p from the scattering data, one must determine or assume a form for $\partial R/\partial k$. If one wished $\partial R/\partial k$ could be calculated in a manner similar to the technique used in Sec. II. The expectation that the final-state effects will be small suggests that results of sufficient accuracy could be obtained by just assuming a convenient form for $R(k, V_k\Omega)$ rather than investing in a long, cumbersome evaluation of $\partial R/\partial k$. The authors choose to assume a Gaussian form for $R(k, V_k t)$,

$$R(k, V_k t) = e^{-(V_k t)^2/\Gamma}, \tag{37}$$

which when Fourier transformed yields

$$R(k, V_k\Omega) = [(\pi\Gamma)^{1/2}/V_k]\, e^{-\Omega^2\Gamma/4}. \tag{38}$$

This form leads to a considerable simplification of Eq. (36). From the results of Sec. II it is obvious that a Γ may be chosen to yield the correct width and qualitatively the correct shape to mimic the $R(k, V_k\Omega - V_k p)$ evaluated in that section. From Fig. 5 it can be seen that the width of $R(k, V_k t)$ in terms of $V_k t$ changes by approximately 8% as k goes from $k = 14.3$ to 28.6 Å^{-1}. It therefore appears safe to assume that Γ changes negligibly over the range of k values which are significant for the experimental data being analyzed. Taking Γ as independent of k and inserting Eq. (38) into (36) yields

$$\int_{-\infty}^{\infty} dp\, p n_p R(k, V_k\Omega - V_k p) \approx -4\pi^2 \rho V_k \left[\left(\frac{\partial S^{NC}}{\partial \omega}\right)_\theta + \frac{S^{NC}}{k}\left(\frac{\partial k}{\partial \omega}\right)_\theta\right] \Big/ \left[1 - V_k\left(\frac{\partial k}{\partial \omega}\right)_\theta\left(1 + \frac{\Omega}{k}\right)\right], \tag{39}$$

where approximate equality $\approx$ is indicated to emphasize that this equation is based on the assumed Gaussian form of $R(k, V_k t)$.

The results of Sec. III may now be reexamined using Eq. (39). In that section the right-hand side (RHS) of the above equation was identified as equal to Ωn_Ω, refer to Eq. (23) and Fig. 8, rather than the convolution of R with pn_p. From the general shape of R one would expect that the convolution of R with pn_p would be broader with less well defined features than pn_p. This means, for example, that the actual single-particle momentum distribution may have a noticeably sharper peak in the vicinity of $p \approx 0.7$ Å than indicated in Fig. 8.

It is somewhat easier to make a quantitive correction for final-state effects on our assessment of the off-diagonal one-particle density matrix. The results for this density matrix presented in Sec. III, Fig. 9, were obtained from

$$\tilde{\rho}_1(0, r) = \frac{1}{4\pi^2}\int_{-\infty}^{\infty} d\Omega \sin\Omega r \ \text{[RHS of Eq. (39)]}. \tag{40}$$

In the impulse approximation the RHS of Eq. (39) is Ωn_Ω [refer to Eq. (23)] and in that approximation $\tilde{\rho}_1$ is quickly shown to be equal to the off-diagonal density matrix $\rho_1(0, r)$. In the present approximation in which $R(k, V_k t)$ is assumed to be a Gaussian, the RHS of Eq. (39) is taken as $\int_{-\infty}^{\infty} dp\, pn_p \times R(k, V_k\Omega - V_k p)$ and Eq. (40) becomes

$$\tilde{\rho}_1(0, r) = \rho_1(0, r) R(k, V_k t = r),$$

where $\tilde{\rho}_1(0, r)$ is the result of the calculation contained in Fig. 9 and $\rho_1(0, r)$ is the "true" density matrix. Figure 10 presents the results obtained from $\rho_1(0, r)$ under the assumption that $R(k, V_k t)$ is a Gaussian with $\Gamma = 53.5$ Å^2, the value of Γ being chosen to give a fit to the experimental data comparable to the fit afforded by the condensate (fourth) term of Eq. (2).

Figure 10 has been drawn assuming that the condensate fraction n_0 is 0.11. If a significantly smaller value had been chosen for n_0; for example, $n_0 = 0.024$, a value more consistent with the previous results; then the resulting $\rho_1(0, r)$ would have negative values for $r \approx 6$ Å. This would be incompatable with the assumption that the wave function of the helium is everywhere non-negative, a zero-temperature assumption utilized in Sec. II to obtain $R(k, V_k t)$. Noting that $\rho_1(0, r)$ was evaluated from data taken at a temperature 1.2°K, the negative portions of the density might be a real temperature effect, implying significant deviations of ρ_1 from its ground state shape due to population of excited states. Another, probably more plausible, explanation may be that the negative values were artifically introduced by errors arising from the finite accuracy of the data and the computational procedure used in the analysis. For example, theoretical calculations indicate that $n_p \propto 1/p$ for small p.[12] It is impractical to expect an experiment of the type being discussed to detect this feature. Adding a term to n_p which behaved as $1/p$ for small p would tend to add a positive contribution to $\rho(0, r)$ which would diminish the size of the negative values of the density matrix.

V. DISCUSSION AND CONCLUSIONS

In this work we have tried to make an honest calculation of the effect of final state interactions on thermal neutron scattering from superfluid He^4 to compare with the Mook-Scherm-Wilkinson (MSW) experiment. These effects are contained in the function $R(k, t)$ and we make no *a priori* assumptions on its shape. However, as described elsewhere[6] we do approximate the exact $R(k, t)$ by Eq.

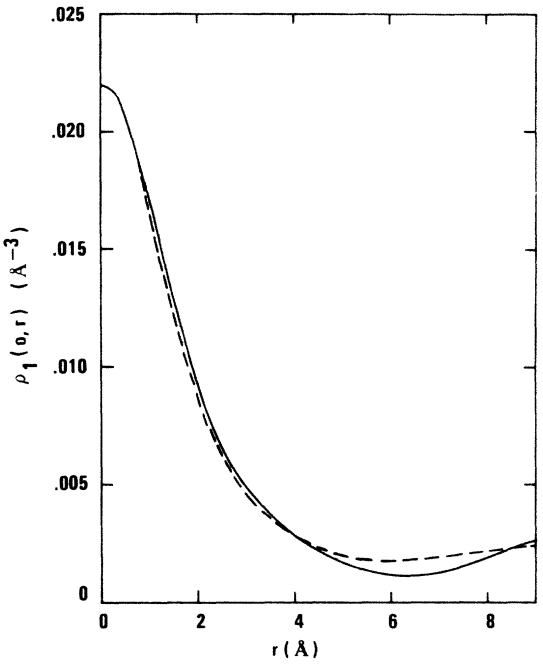

FIG. 10. Off-diagonal one-particle density matrix: solid line, obtained from 1.2 °K data corrected for final-state effects; dashed-line, obtained from 1.2 °K data with no final-state corrections.

(5), which accounts for multiple binary collisions of that helium atom struck by the neutron with other helium atoms, the latter treated independent of each other during their interaction with the struck helium atom. This binary collision approximation neglects the effects of clustering between the passive helium atoms. One other approximation in addition to the binary collision hypothesis is contained in the expression for $R(k, t)$ given by Eq. (5). This consists in the neglect of the motion of a passive helium atom while interacting with the helium atom struck by the neutron. Another approximation utilized in evaluating $R(k, t)$ of Eq. (5) consists of representing in only a crude fashion the off-diagonal two-particle density matrix ρ_2 appearing in $R(k, t)$. This ρ_2 forms the weight function for configurations of initial $(\vec{r})$ and final $(\vec{r}+\vec{V}_k t)$ relative coordinates of struck and passive helium atoms. We believe that these two above-mentioned approximations do not alter the qualitative shape of the scattering cross section. However, a better treatment of either one could change its quantitative aspects. Since there seems to be qualitative agreement between the present theory and the MSW experiment concerning the structure in the condensate contribution to the scattering, it would be quite interesting if the experimental uncertainties in the condensate shape could be even further reduced, thus providing information on the quantitative deficiencies described above.

If our present results are correct, very little relative sharpening of condensate over noncondensate scattering is gained by experimentally feasible increases in neutron momentum transfer. A previous prediction of ours[13] which came to an opposite conclusion in this regard is incorrect, due to inadequate treatment of the strong repulsive forces between the helium atoms in the earlier work.

In view of the relative insensitivity of the shape of the condensate portion of the scattering to neutron momentum transfer k, it may be more profitable for future experiments, to consider varying not k, but rather the absolute temperature T of the superfluid. It has usually been judged that the condensate fraction $n_0(T)$ slowly decreases with increasing T (in a way similar to the known temperature dependence of the superfluid fraction) so that its value at $T \cong 1.2°\mathrm{K}$ is only a bit less than its value at $T = 0°\mathrm{K}$. However, there is, to our knowledge, no satisfactory proof of such temperature behavior of $n_0(T)$. Therefore it appears worthwhile to consider appreciably reducing the superfluid temperature.

We have no good explanation for our predicted shift in the peak of the scattering toward energies higher than the free-particle peak. This result is contradicted by both the experimental observation, as well as other theoretical estimates. For example, phenomenological forms for $S(k, \omega)$ which are adjusted to agree with estimates of its third frequency moment predict the experimentally observed peak shift to lower energies. It is somewhat curious to note that the approximation evaluated here formally satisfies the third and lower moments of the incoherent (self-) contribution to the dynamic structure.

Hohenberg and Platzman's original proposal of the use of high-energy neutron scattering to observe the condensate[14] accounts for final-state broadening of the condensate contribution to the scattering by introducing a "lifetime" effect as an imaginary part of the single-particle energy $\mathcal{E}_k$,

$$\mathrm{Im}\,\mathcal{E}_k = V_k \rho \sigma_{\mathrm{tot}} .$$

The theory employed here makes contact with this phenomenological theory for large times, as may be seen by examining Eqs. (3), (4), (17), and (19). As observed previously, this agreement holds imperfectly even at large times, and breaks down completely for short to moderate times. A significant result is that the effect of final-state interactions is not to just broaden the condensate part of the scattering into a Gaussian or Lorentzian shape, but instead to broaden the condensate into a function $n_0 R(k, V_k \Omega)$ with some structure. This observation does not rest solely on the results of the calculation discussed in Sec. II, which as discussed above may be faulted for using a crude approximation to the off-diagonal two-particle density matrix. The observation that Gaussian or Lorentzian is deficient is substantiated by noting that for the incoherent part of the dynamic structure factor to be given in the form of Eq. (3), the zeroth and third moments of $R(k, \omega - \omega_k)$ must be nonzero while its first and second moments must vanish. These features cannot be obtained with Gaussian or Lorentzian line shapes and may provide some indication that the structure in the experimental scattering data around 101 and 111 meV could be contributed by the condensate.

The most direct way to compare this theory to experiment would be to take theoretical results for the momentum distribution, for example McMillan's Monte Carlo calculation[7]; convolute this distribution with the function R and thereby produce a prediction of the energy dependence of the scattering for comparison with experiment. We in fact originally proceeded along these lines, however it soon became apparent that the use of McMillan's momentum distribution in this theory would yield results for the dynamic structure factor outside the experimental error of the MSW

measurements. One could attribute this failure to the theory presented here, the Monte Carlo momentum distribution, the experimental results, or some combination of these three.

Since this direct approach proved unsatisfactory, we chose to use the theory developed here and the experimental data to determine a single-particle momentum distribution. This approach forces one to decompose the dynamic structure into a condensate and a noncondensate contribution. Treating the momentum distribution as an unknown function makes this decomposition nontrivial. This problem was settled, somewhat arbitrarily, by taking the empirical fit given by Eq. (2) and the decomposition it implies as the correct representation of the dynamic structure factor. Ignoring the complexities introduced by the experimental resolution, the constant k to constant scattering angle transformation, and final-state effects on the noncondensate; the empirical fitting procedure may be thought of as simultaneously choosing a set of parameters A_7, A_8, A_9, B_1, B_2, B_3, and B_4 so that the function $A_7 \exp[-(\omega - A_8)^2/A_9^2]$ yields the best fit to the condensate part of the scattering while the function $B_1 \exp[-(p/B_2)^2] + B_3 p^2 \exp[-(p/B_4)^4]$ is adjusted to give the best fit to the noncondensate momentum distribution. In support of the procedure, the width (4.92 meV, refer to Table I) of the best-fitting Gaussian to the condensate contribution is in rough agreement with the theoretical assessment of the condensate contribution, refer to Fig. 6. On the detrimental side, the function used to fit the noncondensate momentum distribution was chosen arbitrarily. It is quite likely that this function is grossly deficient for small values of the momentum p, while being more acceptable for moderate values of p. Considering the sensitivity of the quantitative results on the assumed form of the momentum distribution and the condensate contribution, we cannot claim confidence in much of the detailed, quantitative results of this analysis. We do have confidence in the following qualitative and semiquantitative results:

(i) The final-state effects in liquid helium include physical mechanisms which do broaden the condensate contribution to the dynamic structure factor so that its FWHM is approximately 5 meV for the conditions corresponding to the MSW experiment. The (final-state-broadened) condensate contribution has structure and is most probably not positive definite.

(ii) A condensate fraction of approximately 2.4% is compatible with the MSW experimental data.

(iii) There is preferential occupation of the momentum states near $p \approx 0.7$ Å^{-1} at temperatures both above and below the λ transition.

APPENDIX A

This Appendix gives a derivation of the function $P(\omega)$ of Eq. (30), which approximately represents the deconvoluted form of the term $A_4 \exp\{-[(\omega - A_5)/A_6]^4\}$ in Eq. (25), a part of the empirical fit to the scattering data. $P(\omega)$ is obtained by taking the first five terms of the following series:

$$\sum_{n=0}^{\infty} \frac{1}{n!} \left(\frac{-\Gamma}{4}\right)^n \frac{d^{2n}}{d\omega^{2n}} A \exp\{-[(\omega - A_5)/A_6]^4\} . \tag{A1}$$

This is in turn based on the claim that

$$f(\omega) = \lim_{\gamma \to -1^+} \sum_{n=0}^{\infty} \frac{1}{n!} \left(\frac{\gamma\Gamma}{4}\right)^n \frac{d^{2n}F(\omega)}{d\omega^{2n}} \tag{A2}$$

is a solution to

$$F(\omega') = (\pi\Gamma)^{-1/2} \int_{-\infty}^{\infty} d\omega f(\omega) e^{-(\omega-\omega')^2/\Gamma} \tag{A3}$$

for sufficiently well-behaved functions $F(\omega)$. To demonstrate that Eq. (A2) is a solution to Eq. (A3) consider the function

$$R_\gamma(\omega - \omega') = [\pi\Gamma(1+\gamma)]^{-1/2} \exp\left(\frac{-(\omega-\omega')^2}{\Gamma(1+\gamma)}\right) . \tag{A4}$$

Expand R_γ in a Taylor's series about $\gamma = 0$:

$$R_\gamma(\omega - \omega') = (\pi\Gamma)^{-1/2} \sum \frac{\gamma^n}{n!} \frac{\partial^n}{\partial\gamma^n} \times \left((1+\gamma)^{-1/2} \exp\left(\frac{-(\omega-\omega')^2}{\Gamma(1+\gamma)}\right)\right) , \tag{A5}$$

where in this and subsequent equations n will be used as the summation index running from 0 to ∞. Note that

$$\frac{\partial}{\partial\gamma} (1+\gamma)^{-1/2} \exp\left(\frac{-(\omega-\omega')^2}{\Gamma(1+\gamma)}\right) = \frac{\Gamma}{4} \frac{\partial^2}{\partial\omega^2} (1+\gamma)^{-1/2} \exp\left(\frac{-(\omega-\omega')^2}{\Gamma(1+\gamma)}\right) . \tag{A6}$$

By an obvious inductive argument

$$\frac{\partial^n}{\partial\gamma^n} (1+\gamma)^{-1/2} \exp\left(\frac{-(\omega-\omega')^2}{\Gamma(1+\gamma)}\right) = \left(\frac{\Gamma}{4}\right)^n \frac{\partial^{2n}}{\partial\omega^{2n}} (1+\gamma)^{-1/2} \exp\left(\frac{-(\omega-\omega')^2}{\Gamma(1+\gamma)}\right) . \tag{A7}$$

Therefore,

$$R_\gamma(\omega - \omega') = (\pi\Gamma)^{-1/2} \sum \frac{1}{n!} \left(\frac{\gamma\Gamma}{4}\right)^n \frac{\partial^{2n}}{\partial\omega^{2n}} \times \exp\left(\frac{-(\omega-\omega')^2}{\Gamma}\right) . \tag{A8}$$

As is well known, R_γ forms a δ sequence as γ approaches -1, therefore

$$\delta(\omega-\omega') = \lim_{\gamma\to -1} (\pi\Gamma)^{-1/2} \sum \frac{1}{n!}\left(\frac{\gamma\Gamma}{4}\right)^n \frac{\partial^{2n}}{\partial\omega^{2n}} \times \exp\left(\frac{-(\omega-\omega')^2}{\Gamma}\right) . \quad \text{(A9)}$$

Treating $F(\omega')$ as a known function, write

$$F(\omega') = \int_{-\infty}^{\infty} d\omega\, \delta(\omega-\omega')F(\omega) . \quad \text{(A10)}$$

Representing the δ function by the δ sequence given in Eq. (A9) yields

$$F(\omega') = \lim_{\gamma\to -1} (\pi\Gamma)^{-1/2} \int_{-\infty}^{\infty} d\omega F(\omega) \times \sum \frac{1}{n!}\left(\frac{\gamma\Gamma}{4}\right)^n \frac{\partial^{2n}\exp[-(\omega-\omega')^2/\Gamma]}{\partial\omega^{2n}} . \quad \text{(A11)}$$

Assuming that $F(\omega)$ is sufficiently well behaved to allow term-by-term integration, integrate by parts to obtain

$$F(\omega') = \lim_{\gamma\to -1} (\pi\Gamma)^{-1/2} \sum \frac{1}{n!}\left(\frac{\gamma\Gamma}{4}\right)^n \times \int_{-\infty}^{\infty} d\omega \left[\exp\left(\frac{-(\omega-\omega')^2}{\Gamma}\right)\right] \frac{d^{2n}F(\omega)}{d\omega^{2n}} , \quad \text{(A12)}$$

where it is assumed that the boundary terms vanish, i.e.,

$$\lim_{|\omega|\to\infty} e^{-\omega^2/\Gamma} \frac{d^m F(\omega)}{d\omega^m} = 0$$

for all integers m. Again assuming that limit and summation may be interchanged with the integration operation

$$F(\omega') = (\pi\Gamma)^{-1/2} \int_{-\infty}^{\infty} d\omega \left[\lim_{\gamma\to -1^+} \sum \frac{1}{n!}\left(\frac{\gamma\Gamma}{4}\right)^n \frac{d^{2n}F(\omega)}{d\omega^{2n}}\right] \times \exp\left(\frac{-(\omega-\omega')^2}{\Gamma}\right) , \quad \text{(A13)}$$

which demonstrates that the expression in large square brackets,

$$f(\omega) = \lim_{\gamma\to -1^+} \sum \frac{1}{n!}\left(\frac{\gamma\Gamma}{4}\right)^n \frac{d^{2n}F(\omega)}{d\omega^{2n}} ,$$

is a solution to

$$F(\omega') = (\pi\Gamma)^{-1/2} \int_{-\infty}^{\infty} d\omega f(\omega) \exp\left(\frac{-(\omega-\omega')^2}{\Gamma}\right) .$$

The above derivation of the form of the deconvoluted function $f(\omega)$ from the experimental data $F(\omega)$ is clearly not rigorous, since it has not been demonstrated that $F(\omega)$ behaves smoothly enough to validate the interchange of orders of integration, summation, and limit. However, our five term approximation $f(\omega)$ in Eq. (30) of the text [there called $P(\omega)$] is clearly a very good numerical solution, as Fig. 7 indicates.

---

*Research sponsored jointly by the National Science Foundation and by the U. S. Atomic Energy Commission under contract with the Union Carbide Corporation.

†Portions of this work are taken from a Ph. D. thesis submitted by L. J. Rodriguez to the Georgia Institute of Technology, 1973.

[1]L. Van Hove, Phys. Rev. 95, 249 (1954).

[2]R. D. Puff and J. S. Tenn, Phys. Rev. A 1, 125 (1970).

[3]H. A. Mook, R. Scherm, and M. K. Wilkinson, Phys. Rev. A 6, 2268 (1972).

[4]The data as presented in Ref. 3 and here are proportional to the dynamic structure factor $S(k,\omega)$ broadened by an experimental resolution function with a FWHM of approximately 2.1 meV.

[5]After examining Fig. 2, one might be tempted to try to obtain a better fit to the 4.2 °K data around the three points near the peak. The straightforward way to accomplish this is to add an additional function, for example a Gaussian, to Eq. (2) and to redo the least-squares analysis with the resulting 4 terms of the new Eq. (2) (recall that $A_7 \equiv 0$ at 4.2 °K). We estimate graphically that an amplitude of $\sim\frac{1}{2}$ count and a full width of 2–3 meV, would be adequate. This additional function would be interpreted as part of the noncondensate contribution. To complete the analysis, one would fit the 1.2 °K data with the same function with a condensate term added, i.e., five terms taking $A_7 \neq 0$. It is evident, after noting the anticipated size of the added noncondensate term, that the final result for the condensate fraction would be somewhat less than 2.4%. Some of the results of the further analysis reported in this work would also be modified by this program; but, in the author's opinion, by an uninterestingly small amount.

[6]H. A. Gersch and L. J. Rodriguez, Phys. Rev. A 8, 905 (1973).

[7]W. L. McMillan, Phys. Rev. 138, A442 (1965).

[8]R. Feltgen, H. Pauly, F. Torello, and H. Vehmeyer, Phys. Rev. Lett. 30, 820 (1973).

[9]Arguments in support of this judgement are advanced by H. A. Gersch and P. N. Smith, Phys. Rev. A 4, 281 (1971).

[10]An attempt at including effects of the attractive part of the helium-helium potential in $f(r)$ is reported by R. D. Murphy [Phys. Rev. A 5, 331 (1972)]. He used the form $f(r) = \exp[-(a/r)^n \pm (a/r)^m]$, where the plus sign in front of the second term in the exponential

would correspond to attractive interactions. He finds that the negative sign yields superior results. However, using the same range parameter a for both repulsive and attractive terms is highly artifical and is not strong evidence against the appearance of an effect of the attractive part of the potential in $f(r)$.

[11]D. Schiff and L. Verlet, Phys. Rev. 160, 208 (1967).

[12]O. K. Harling, Phys. Rev. Lett. 24, 1046 (1970); A. G. Gibbs and O. K. Harling, Phys. Rev. A 3, 1073 (1971).

[13]H. A. Gersch, L. J. Rodriguez, and P. N. Smith, Phys. Rev. A 5, 1547 (1972).

[14]P. C. Hohenberg and P. M. Platzman, Phys. Rev. 152, 198 (1966).